Preliminary Investigation of Wake Vortex Generated by Spinning Quadrotor Propellers Using Overset Mesh

Joshua Christian Nathanael[1] and C. H. John Wang[2]
Air Traffic Management Research Institute (ATMRI), Nanyang Technological University
65 Nanyang Drive, Singapore 637460

Kin Huat Low[3]
School of Mechanical and Aerospace Engineering, Nanyang Technological University
50 Nanyang Avenue, Singapore 639798

As unmanned aircraft or drones are becoming more commonplace in our ever-developing environment where a number of drones can be flying in the same given airspace, a drone is likely to experience wake vortex turbulence from another drone nearby. Therefore, there is a need to understand how the airflow is generated from one vehicle and to what extent this airflow might affect another vehicle. Results of such studies will be useful in establishment of safe separation of drone operations. In the present work, flow simulations are carried out using overset mesh on ANSYS Fluent 19.2 for both single and multiple propellers, and the flights in hovering and forwarding motion are considered. The simulation results obtained are in general agreement to the experimental results that are available from other studies. This provides support to the idea that the method of flow simulation can be acceptably reliable in predicting the resulting airflow from a flying drone and the proposed method can be further applied to various cases of drone flights.

Nomenclature

D	=	Diameter of propeller
R	=	Radius
V_z	=	Velocity in Z-direction
ω	=	Angular velocity
r	=	Radial position
T	=	Thrust
ρ	=	Density of air
n	=	Angular velocity in rotations per second

I. Introduction

The world has seen an increase in the use of unmanned aircraft or drones in recent years, with their current applications varying [1] from search and rescue [2], pesticide spraying [3], to meteorology measurements [4], and possible applications of drones in the future including food delivery [5] and cargo transport [6]. As drones are becoming more commonplace in our ever-developing environment where a number of drones can be flying in the same given airspace, a drone is likely to experience wake vortex turbulence from other nearby drone (Figure 1), and

[1] Project Officer, Unmanned Aerial Systems (UAS) Programme, ATMRI
[2] Research Fellow, Assistant Programme Director, UAS Programme, ATMRI
[3] Professor, School of Mechanical and Aerospace Engineering; e-mail: mkhlow@ntu.edu.sg

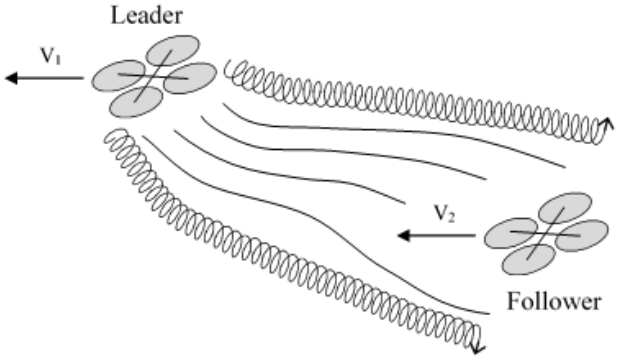

Fig. 1 A drone flying in the wake region of another drone.

the wake vortex turbulence from a leading vehicle can pose hazards such as loss of lift, reduced control authority and induced roll on the following vehicle [7]. Therefore, to be able to establish safe separation of drone operations and ensure the safety of the many drones flying, there is a need to understand how the airflow is generated from one vehicle and to what extent this airflow might affect another vehicle.

While the wake vortex from large fixed-wing and rotorcraft has been investigated thoroughly in the past [8, 9, 10], the studies of the flow from the smaller drones such as the quadrotor have been conducted more recently. The flow from a single rotating propeller has been simulated with Computational Fluid Dynamics (CFD) method in various studies, such as by Kutty and Rajendran [11] and Pérez Gordillo, et al. [12] who used the Multiple Reference Frame (MRF) model, and the method is able to predict the thrust generated by comparing it with the measured thrust from experiments. There are also studies that investigate the effects of rotor-to-rotor interactions for multiple rotating propellers. It has been found that the thrust generated from the propellers fluctuates and decreases average-wise when the propellers are placed close to one another [13, 14, 15], and flow simulations in several studies using SolidWorks Flow Simulation [16], ANSYS Fluent with overset mesh [17], and NASA's OVERFLOW solver with structured overset grids [18] have been shown to be able to predict the reduction in thrust for multiple rotating propellers.

Most studies focus on the case for a quadrotor in hover condition with all the thrusts generated vertically by the propellers, however, only a few that studies the airflow from a quadrotor when it is flying forward. Simulations [19, 20] and a wind tunnel test [4] have been done to do so, however, they focus on the airflow around the quadrotor itself and there has not been much study that investigates what happens to this airflow long after it leaves the quadrotor and how it evolves over time. This study provides insight into the feasibility of using CFD solver as a tool to study the generated airflow from the quadrotor by first having several flow simulations using overset mesh on ANSYS Fluent 19.2 for both single and multiple propellers in different flight conditions and comparing the simulation results with experimental results that are available in other studies. This is to ensure that using the flow simulations can produce reasonable results when the method is further applied to more cases and more flight conditions to study the resulting airflow.

II. Mesh Convergence and Turbulence Model Study

A. Settings for Simulation

In this part of the study, mesh convergence study is carried out to find the minimum number of cells above which the simulations results are invariant, and the turbulence model study is carried out to choose which turbulence model is able to simulate the flow from a rotating propeller most accurately. The flow simulations use a propeller of 16 inches diameter and 4 inches pitch as shown in Figure 2(a), the 3D CAD model of which was generously provided by Prof. Ali Türker Kutay of Middle East Technical University who had used it in several of his studies [2, 13].

The flow simulations use overset mesh that require overlapping of the Farfield mesh as the background zone and the Rotating mesh as the component zone, and the latter contains the propeller surface which is set as a non-slip wall. The Farfield and the Rotating meshes are created separately using the ANSYS Meshing module from the ANSYS Workbench with the domain sizes and lengths following that of [17] as shown in Figure 2(b). The boundary conditions of the Farfield mesh follow that of [12], where the upper and side surfaces of the Farfield are pressure inlets and the lower surface of the Farfield is a pressure outlet, and their settings are kept as default.

In Ref. [17], the flow simulations use different air properties as they validated their thrust prediction with experiments conducted in their locale with high elevation, and so in this study for the simulation of a single propeller

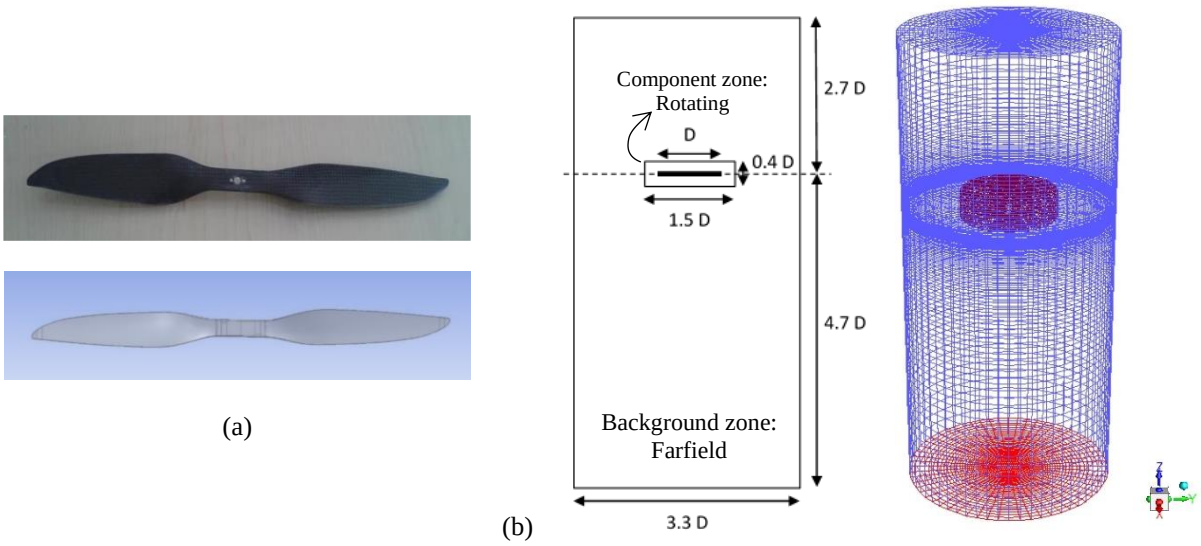

(a) (b)

Fig. 2 Models considered: (a) Picture and CAD model of the 16x4 Propeller from [2, 13] (top) and its CAD model imported into ANSYS Workbench (bottom); (b) Dimensions for the Farfield and Rotating meshes (left) and the resulting meshes as viewed in Fluent (right).

in hover, the density and dynamic viscosity of the air is changed to 0.888 kg/m^3 and 1.8029e-05 kg/ms, respectively, to follow [17].

Apart from the varying turbulence model part in this study, all of the flow simulations use the k-ω Shear Stress Turbulence (SST) turbulence model with curvature correction, as it is one of the most commonly used turbulence model for simulating flow from a rotating propeller [11, 12, 17] and it is not as computationally expensive as Detached Eddy Scale (DES) or Large Eddy Scale (LES) simulation. In the solution methods setting of ANSYS Fluent, only the Coupled pressure-velocity coupling scheme that is compatible with the overset mesh. For the spatial discretization, the Least-Squares Cell Based scheme is used for the gradient, Second Order for the pressure, Second Order Upwind for the Momentum, the Turbulent Kinetic Energy and the Specific Dissipation Rate.

The angular velocity of the rotating propeller is chosen to be 3000 rpm. For each case, the calculations are done in two parts: the first part is done with a steady-state solver with the Pseudo Transient option turned on and Frame Motion is applied to the Rotating mesh until the residuals are lowered to 1e-04; and then the calculations are continued in a transient solver with Mesh Motion applied to the Rotating mesh, the time discretization scheme of First Order Implicit and the time step of 0.0001 seconds until the flow time of one second is reached. Unsteady simulation is required in this study to accurately simulate the flow from the rotating propeller and the results from the steady state calculation only become the initial solution at the start of the transient calculation.

Note that it is imperative that the flow solver is set to double precision when using the Overset library, as the accurate identification of the moving and far-field zones are dependent on having high precision cell position data.

B. Mesh Convergence Study

The mesh convergence study is conducted by first varying the mesh density of the Rotating zone while keeping the Farfield mesh constant with “Farfield-Coarse”; this is followed by varying the mesh density of the Farfield mesh while keeping the Rotating zone constant with “Rotating-Medium”. Table 1 shows the different Rotating and Farfield meshes used in the mesh convergence study. The Rotating zones are created using face sizing with cell inflation, while the Farfield meshes are generated by modifying *Z*-axis resolution while maintaining the same mesh in *XY*-plane

From the *Z*-velocity, i.e. the downward velocity, contours of each case (Figures 3 and 4), the profiles shown in Figure 5 are plotted along a line from the center going outward radially at the height 1*R* below where the propeller is situated. The values of the velocity (V_z) are normalized by dividing them by the propeller’s tip velocity (ωR), and they are compared with the profile presented in the literature [17]. The simulations in the present study yield similar results even when using different meshes and they capture the trend shown in the literature, although the magnitude is overestimated starting from around r = 0.2 R. The overestimation of the velocity magnitude may be due to the difference in the geometry of the propeller built into the setup. The different method in importing the CAD model of the propeller, treating the propeller’s surfaces and incorporating the propeller’s form into the Rotating mesh might

have caused the propeller's geometry in this study to differ slightly than in the literature, and this may affect how the induced flow from the rotating propeller is simulated. On a side note, the values of the normalized velocity from the literature is modified so the tip velocity in the present study is calculated using the propeller's radius, following convention of propeller flow, instead of the diameter from the original paper [17].

Table 1 Various Farfield and Rotating meshes used for the mesh convergence study.

Mesh	Rotating-Coarse	Rotating-Medium	Rotating-Fine
Minimum face size	2.7 mm	2 mm	1 mm
First layer height	(No inflation)	0.04 mm	0.02 mm
Number of layers	(No inflation)	14	18
Y+ value	4.4 to 98.1	0.10 to 5.90	0.051 to 3.21
Number of elements	156,371	816,873	1,626,013

Mesh	Farfield-Coarse	Farfield-Medium	Farfield-Fine
Number of elements	279,000	558,000	837,000

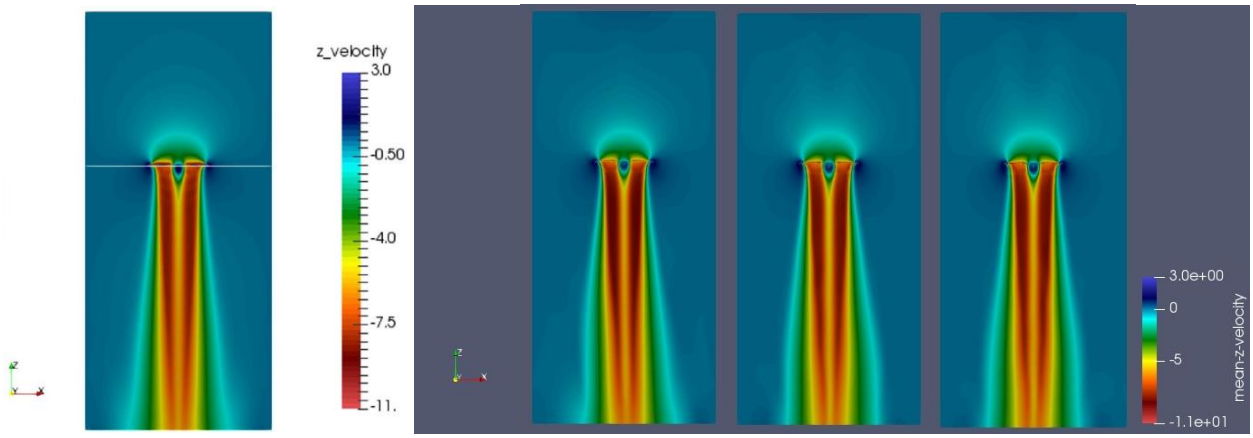

(a) (b)

Fig. 3 *Z*-velocity contour: (a) from literature [17]; (b) from simulation using (left to right) Rotating-Coarse, Rotating-Medium and Rotating-Fine.

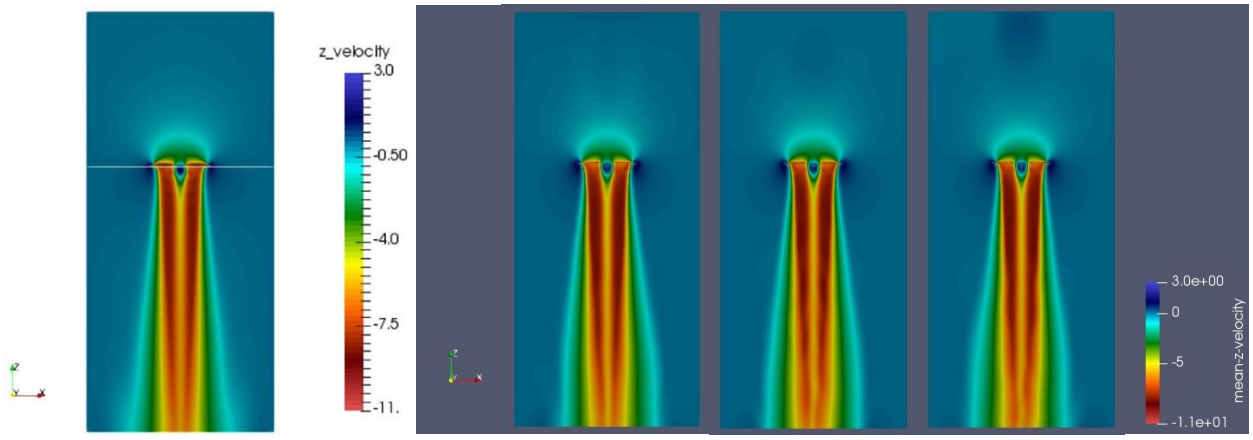

(a) (b)

Fig. 4 *Z*-velocity contour: (a) from literature [17]; (b) from simulation using (left to right) Farfield-Coarse, Farfield-Medium and Farfield-Fine.

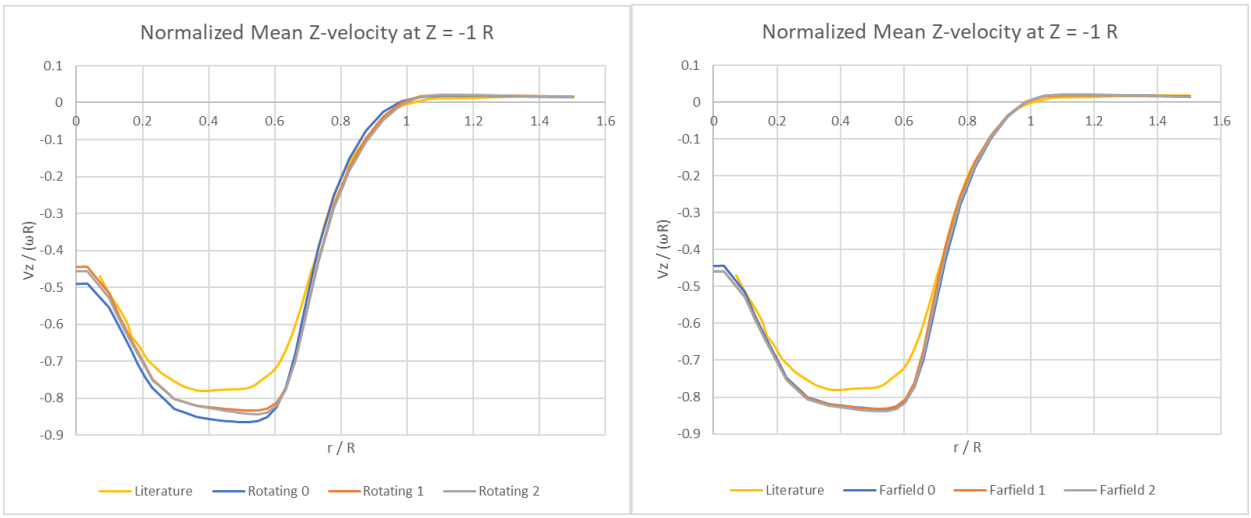

(a) (b)

Fig. 5 Normalized *Z*-velocity plot at *Z* = -1*R*: (a) by Rotating meshes; (b) by Farfield meshes.

C. Turbulence Model Study

In this part of the study, the following turbulence models based on the Reynolds-averaged Navier-Stokes (RANS) equations are used in running the flow simulations with the "Rotating-Fine" and "Farfield-Coarse" meshes: k-ω Shear Stress Turbulence (SST), which is also used in [17], Standard k-ε, and Realizable k-ε. Curvature correction option is turned on for all the turbulence models and the Enhanced Wall Treatment is used for Standard and Realizable k-ε turbulence models. The Spalart-Allmaras turbulence model is not compatible with the overset model in the version 19.2 of ANSYS Fluent, and thus its exclusion from this study.

The *Z*-velocity contours from using different turbulence models are shown in Figure 6 and the plotted *Z*-velocity profiles are shown in Figure 7. The velocity profiles from current simulations are quite similar when the k-ω SST and Realizable k-ε turbulence models are used, and their trend are in agreement with the velocity profile presented in [17] with some overestimation of the magnitude just like in the previous part of the mesh convergence study. On the other hand, the Standard k-ε turbulence model is known to be dissipative when encountering high shear flow, as is the case along the boundary between the downwash and the ambient. This leads to a more spread-out velocity profile compared with the other turbulence models, in that the velocity profile have a reduced peak of Z-velocity at around $r = 0.4\ R$ and in turn an overestimation of the flow velocity at the center from $r = 0$ to $r = 0.2\ R$.

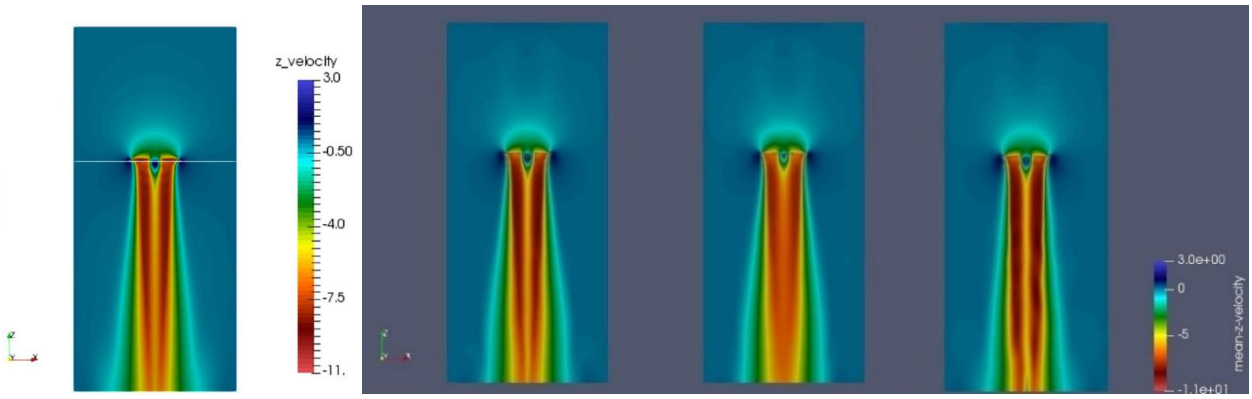

(a) (b)

Fig. 6 *Z*-velocity contour: (a) from literature [17]; (b) from simulation using (left to right) k-ω SST, Standard k-ε, and Realizable k-ε turbulence models.

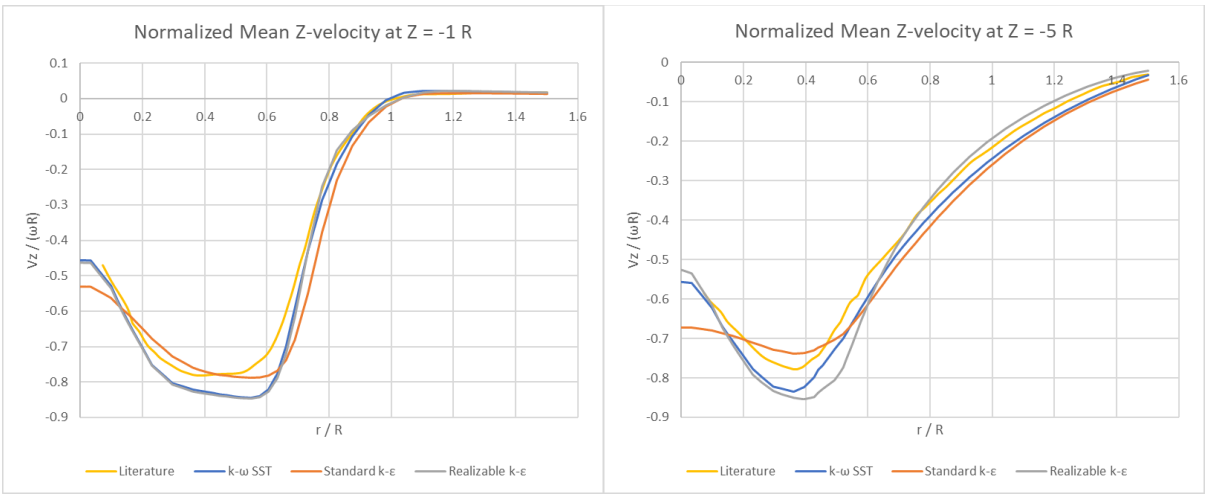

(a) (b)

Fig. 7 Normalized *Z*-velocity plot from using different turbulence models: (a) at *Z* = -1*R*; (b) at *Z* = -5*R*.

III. Comparisons of Multi-Propeller Interference in Hover with Thrust Measurements

A study by Kaya, et al. [13] used four of the 16x4 propellers, along with other types of propellers, to examine the effect of the gap distance between propellers on the resulting thrusts. It is found that the resulting thrusts decreases with decreasing gap distance, and this part of the present study looks into the capability of the CFD method in simulating the flow interactions between multiple propellers and reproducing the effect discovered in the study by Kaya, et al. From the data for 16x4 propeller presented in that study, the angular velocity of 4000 rpm is chosen, and the gap distance of 9 cm and 3 cm are chosen as the measured thrusts differ more significantly between those two gap distances. In creating the mesh for the two cases, only half of the whole domain is built into the setup and a symmetry boundary condition is given for the symmetry plane in the middle, so instead of 4 Rotating meshes, only two are built into the setup to reduce the number of cells and the computational cost of the flow simulation. The two Rotating meshes mirror each other and they rotate in opposite directions for the simulation.

Figure 8(a) shows the dimensions of the Farfield and the Rotating meshes. The Farfield mesh for the multiple propellers in hover is slightly enlarged from the one for a single propeller in hover to ensure adequate distance from the propellers to the side boundaries. The Farfield mesh is also built with a rectangular shape to make easier the application of cell sizing at designated regions. As can be seen in Figure 8(b), the Farfield mesh in the case for 3 cm gap distance has smaller cells in certain areas to ensure enough overlapping cells between the symmetry plane in the Farfield mesh and the propeller surface in the Rotating mesh. A case using a single 16x4 propeller is also run for comparison with cases with multiple propellers, and since there was no information given on the air properties in [13], the flow simulation was run using the default standard air properties at sea-level conditions with density 1.225 kg/m^3 and dynamic viscosity 1.7849e-05 kg/ms. Figure 9 shows the resulting *Z*-velocity contour as viewed from the planes passing through the center of the propellers.

The thrust measurements from the experiment in [13] and the thrust calculations from the simulation in this study are tabulated in Table 2. From the flow simulation, the thrust from a single propeller averages at 8.72 N, the thrust in the case with 9 cm gap distance averages at 8.60 N, and in the case with 3 cm gap distance 8.56 N. There is a reduction of 1.38% in the resulting thrust for the case with 9 cm gap distance and 1.83% for the case with 3 cm gap distance. Meanwhile, from the experiment, the thrust from a single propeller at 4000 rpm is 7.98 N, then with 9 cm gap distance it becomes around 7.87 N per propeller and with 3 cm gap distance 7.62 N per propeller, so there is a thrust reduction of 1.38% when the gap distance is 9 cm and 4.51% when the gap distance is 3 cm.

While the thrust reduction is similar between simulation and experiment for the case with 9 cm gap distance, the more drastic thrust reduction in the experiment for the case with 3 cm gap distance is not successfully replicated in the simulation. This may be due to the use of symmetry boundary condition to build a half-size of the full fluid domain, as Fluent assumes a zero flux of all quantities across the symmetry boundary and the flow velocity normal to the symmetry plane is fixed to be zero. This may have an effect in simulating the flow interaction between propellers which might be more significant and critical for the case with 3 cm gap distance. Furthermore, insufficient mesh resolution could also undermine the higher shear experienced with the smaller gap distance and cause the discrepancy.

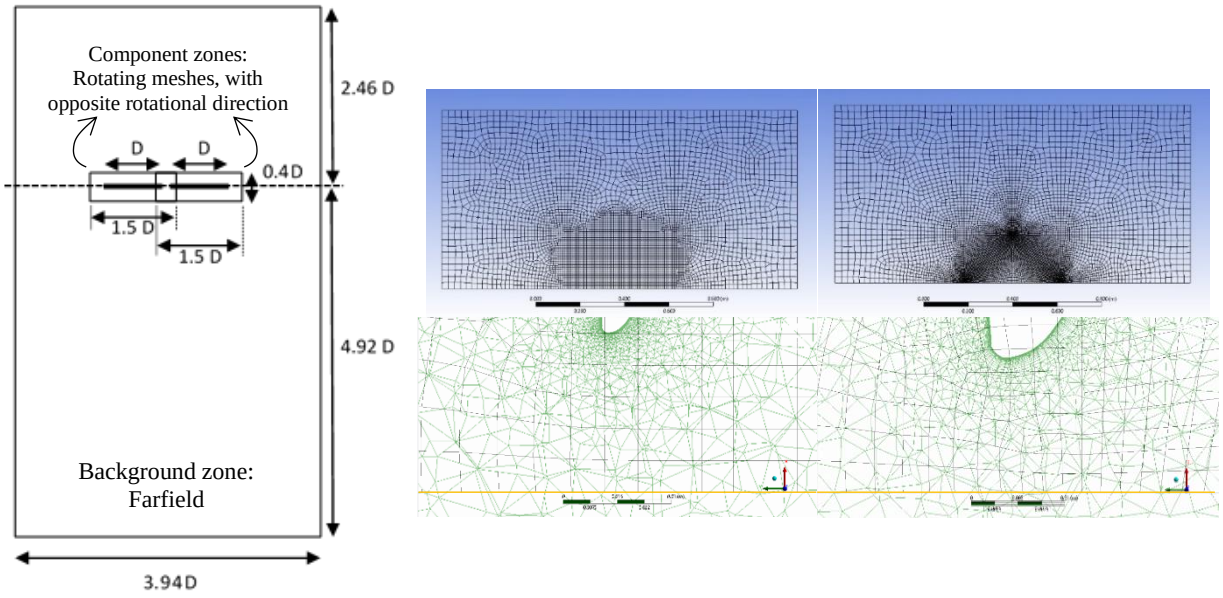

(a) (b)

Fig. 8 Meshes for simulation: (a) Dimensions for the Farfield and Rotating meshes; (b) Farfield mesh (top row) for the case of multiple propellers with 9 cm (left) and 3 cm (right) gap distance and the overlapping cells (bottom row) in the Farfield (black) and Rotating (green) meshes between the symmetry boundary (yellow) and the tip of the propeller.

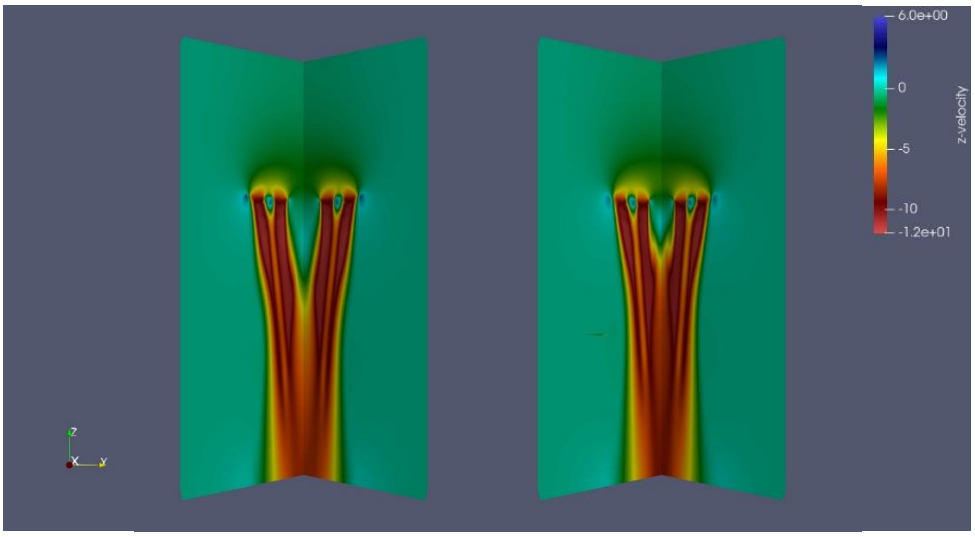

(a) (b)

Fig. 9 *Z*-velocity contour from the simulation: (a) with 9 cm; (b) with 3 cm propellers gap distance.

Table 2 Thrust measurements from experiment [13] and thrust calculations from simulation.

	Single Propeller	Multi-Propeller 9 cm gap distance	Multi-Propeller 3 cm gap distance
Experiment	7.98 N	7.87 N	7.62 N
Thrust Reduction	-	1.38%	4.51%
Simulation	8.72 N	8.60 N	8.56 N
Thrust Reduction	-	1.38%	1.83%

IV. Comparisons with PIV Measurements in Hover Condition

For this part of the study, flow simulation is carried out for a single propeller in hover condition, and the simulation results are compared with Particle Image Velocimetry (PIV) measurements from a study by Zhou, et al. [14]. To follow the experiment conducted by Zhou, et al., another propeller for the simulation is built based on the propeller used in the experiment, as shown in Figure 10(a). Details of the propeller that are given include the cross section of the propeller uses the E63 airfoil as shown in their study, the diameter of the propeller 240 mm (R = 0.12 m), the twist angle at the tip 11.6°, and the twist angle at 0.3R 26.3°. Additionally, the supporting structure used in the experiment is also modelled for the flow simulation in this present study as shown in Figure 10(b), with the length and diameter of the nacelle 72 mm and 34 mm respectively, and the height and diameter of the rod 330 mm and 16 mm respectively.

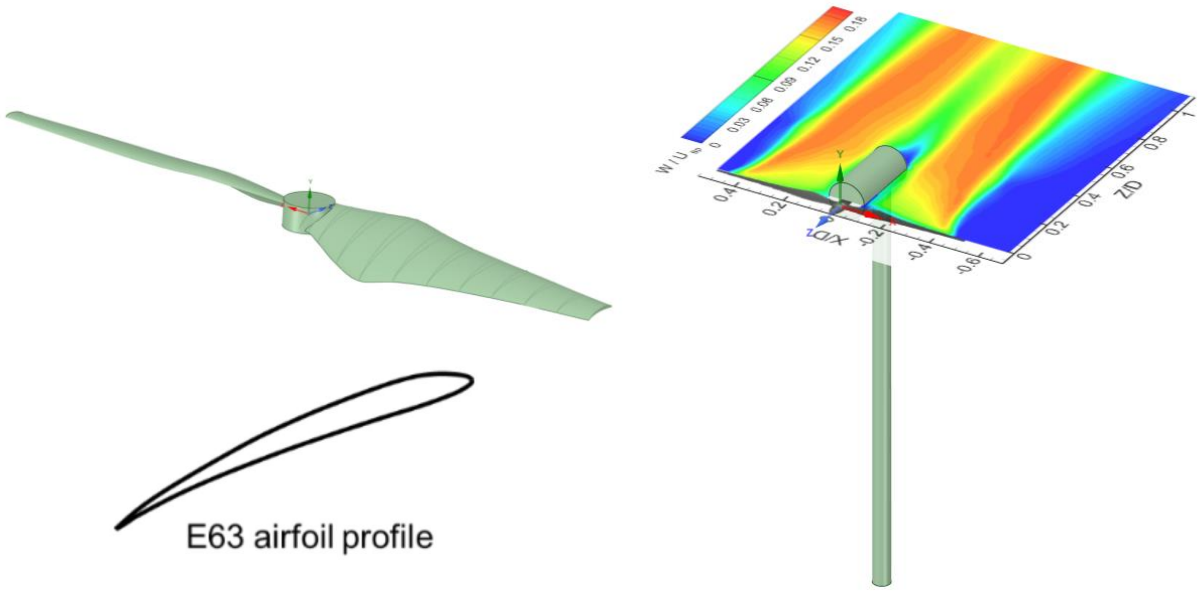

(a) (b)

Fig. 10 Models considered: (a) 240 mm propeller for the present study (top) built using the E63 airfoil section (bottom) from [14]; (b) The supporting structure model used for the simulation.

Two cases of flow simulation are done using this 240 mm propeller with default standard sea-level air properties: one has a single rotating propeller, while the other has two propellers rotating in opposite directions with a gap distance of 12 mm between them. Both cases use the angular velocity of 81 rotations per second, or 4860 rpm. From the simulation, the single rotating propeller generates 2.836 N thrust (Thrust coefficient = $4T/(\rho n^2 D^4 \pi^3)$ = 0.01372), while each of the two counter-rotating propellers generates in average 2.829 N thrust (Thrust coefficient = 0.01370). For comparison, the thrust coefficient for a single rotating propeller as reported in [14] is 0.013.

The flow simulation for the single propeller case is able to produce a similar thrust coefficient, however the generated thrust from each propeller in the simulation for two counter-rotating propellers is 0.998 times the thrust for single rotating propeller. From the experiment of two counter-rotating propellers in [14], the thrust from each of the propeller is 0.984 times the thrust from a single rotating propeller. Even though both propellers are built into the setup for the simulation of two counter-rotating propellers, the predicted thrusts are also not reduced as much as reported from the experiment, thus suggesting that other factors in the simulation setup might be affecting the solver's capability in accurately replicating the interactions between the two propellers.The velocity contour is processed from the flow simulations results and compared with the PIV measurements from [14]. Figure 11 shows the velocity contour as viewed from the top looking down and perpendicular to the flow direction, while Figure 12 shows the velocity contour at 0.024, 0.12 and 0.24 meters downstream from the propeller. The velocity in the flow's direction from the flow simulation is generally in agreement with the PIV measurements, with an apparent effect on one propeller's flow from the other in the case for two counter-rotating propellers. There is however an exaggeration of the induced upwash in the flow simulation results as shown by the added spike-like characteristic in the velocity contour. This may be due to the alignment of the two propellers in the simulation, such that as they are counter-rotating in tandem and the rotational speed is kept constant during the simulation, their tips always get to be in very close proximity in every

rotation and thus possibly causing the exaggerated induced upwash. The lack of cells in the region between the two propellers could also cause the shear stresses from the propeller's induced flow to be calculated inaccurately and thus possibly causing the exaggerated induced upwash.

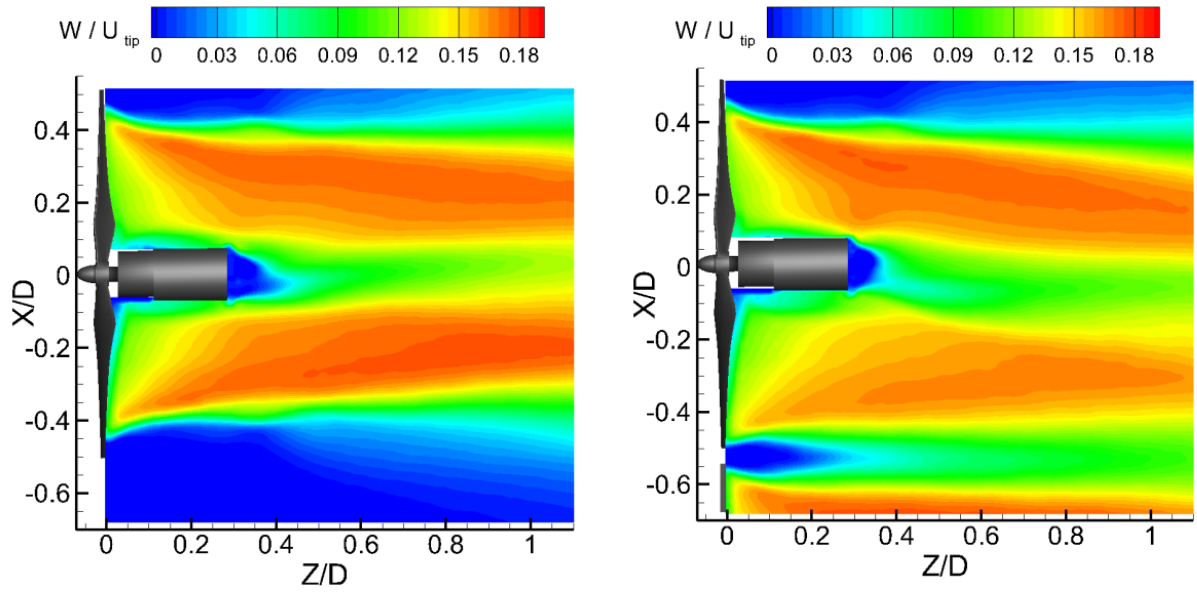

(a)

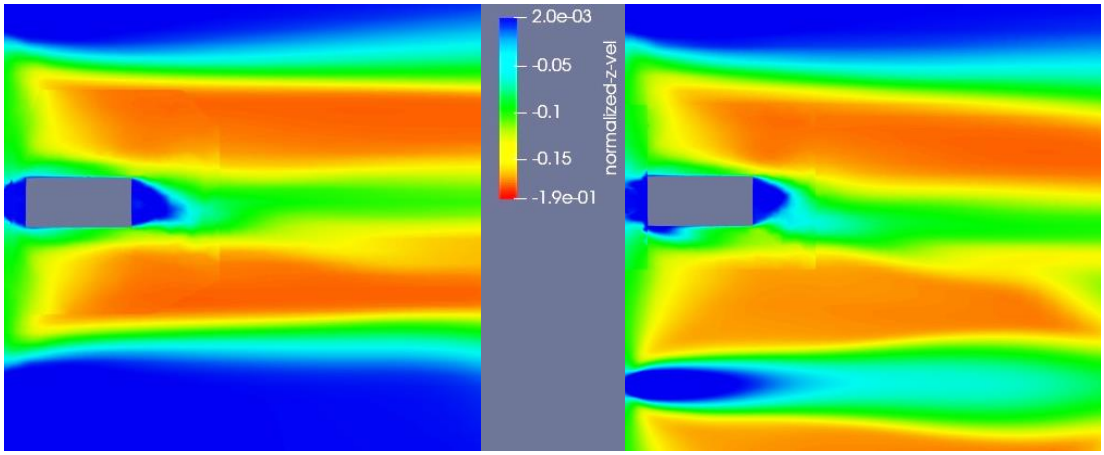

(b)

Fig. 11 Velocity magnitude contour: (a) from PIV measurements [14]; (b) from simulation for a single propeller (left) and two counter-rotating propellers (right).

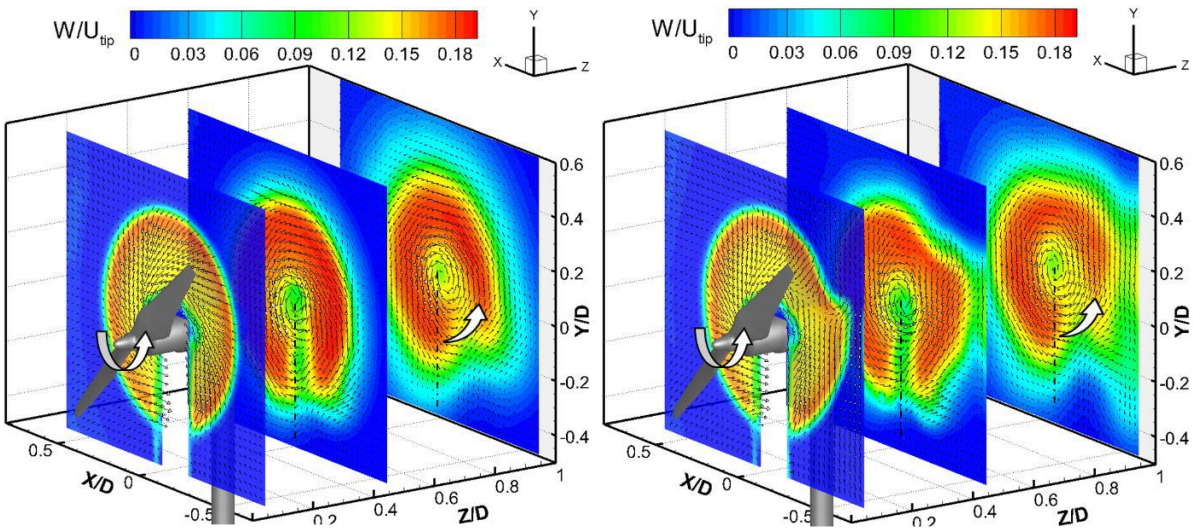

(a)

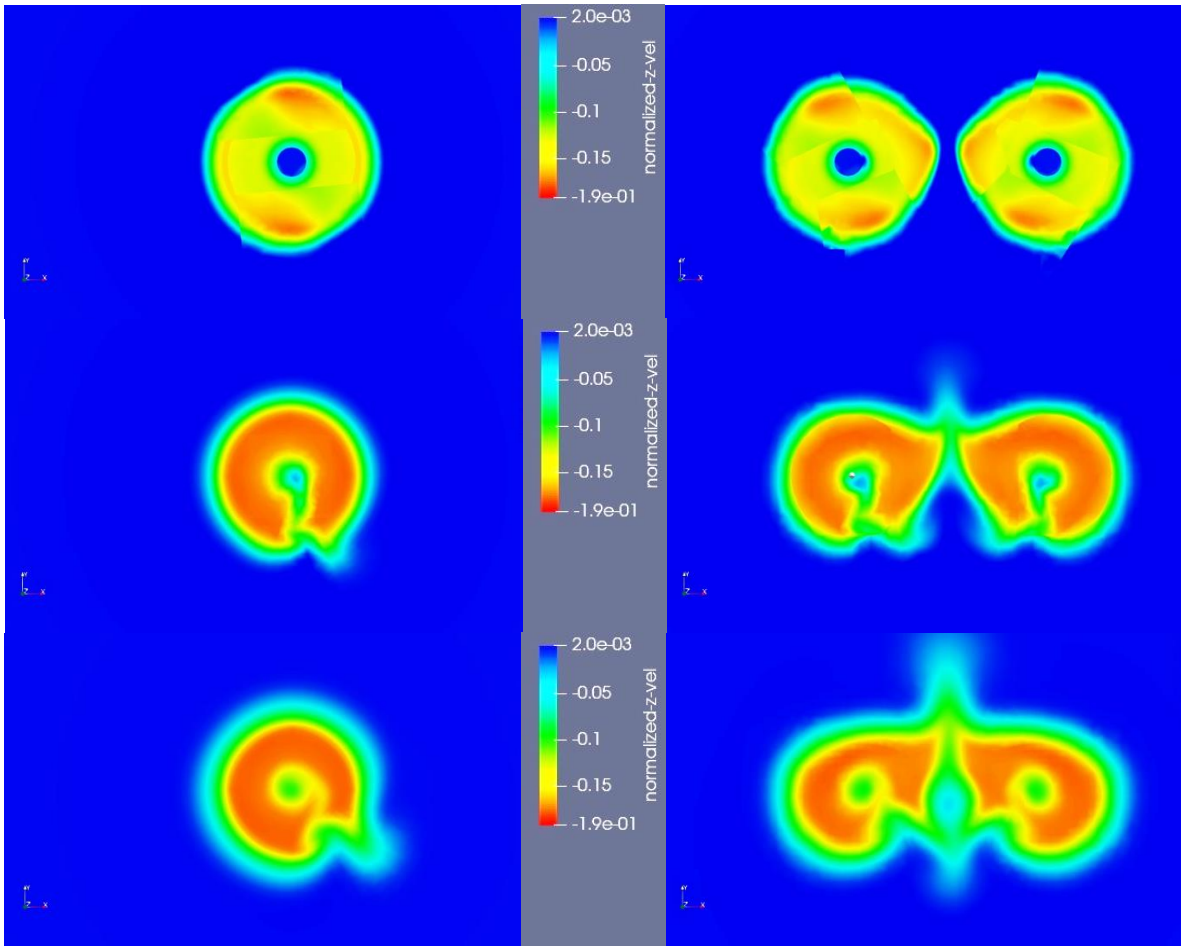

(b)

Fig. 12 Velocity magnitude contour:
(a) from PIV measurements [14] at different downstream positions; (b) from simulation at (top to bottom) 0.024 m, 0.12 m, and 0.24 m downstream from a single propeller (left) and two counter-rotating propellers (right).

V. Comparisons with PIV Measurements in Forward Flight Condition

We next present the flow simulation from a single 240 mm propeller in forward flight and the comparison with PIV measurements from an experiment by Ning, et al. [21]. The Farfield mesh for the forward flight condition is much larger than the one for the hover condition. The Farfield is a cube with the length of each side 4.8 meters, 20 times the propeller's diameter. The boundary conditions of the Farfield mesh follow that of [19] where the front and top boundaries of the Farfield, the highlighted surfaces shown in Figure 13(a), are velocity inlets with the inlet flow velocity 10 m/s in the -*Z*-direction, and the rest of the boundaries are pressure outlets and their settings are kept as default.

The Rotating mesh is in the center of the cube, and instead of modelling the whole supporting structure like in the previous part, only the nacelle below the propeller is included in the setup. Both the propeller and the nacelle are tilted at an 10^o angle as can be seen in Figure 13(b). The angular velocity for the Rotating meshes is chosen to be 5300 rpm based on the measured lift from the propeller in the experiment and the designed lift of 3 N. It should be noted that the propeller used in [21] is reported to have a twist angle of 28.1^o at 0.3R from the center of the propeller instead of 26.3^o, and therefore there is a slight difference with the propeller built for this present study.

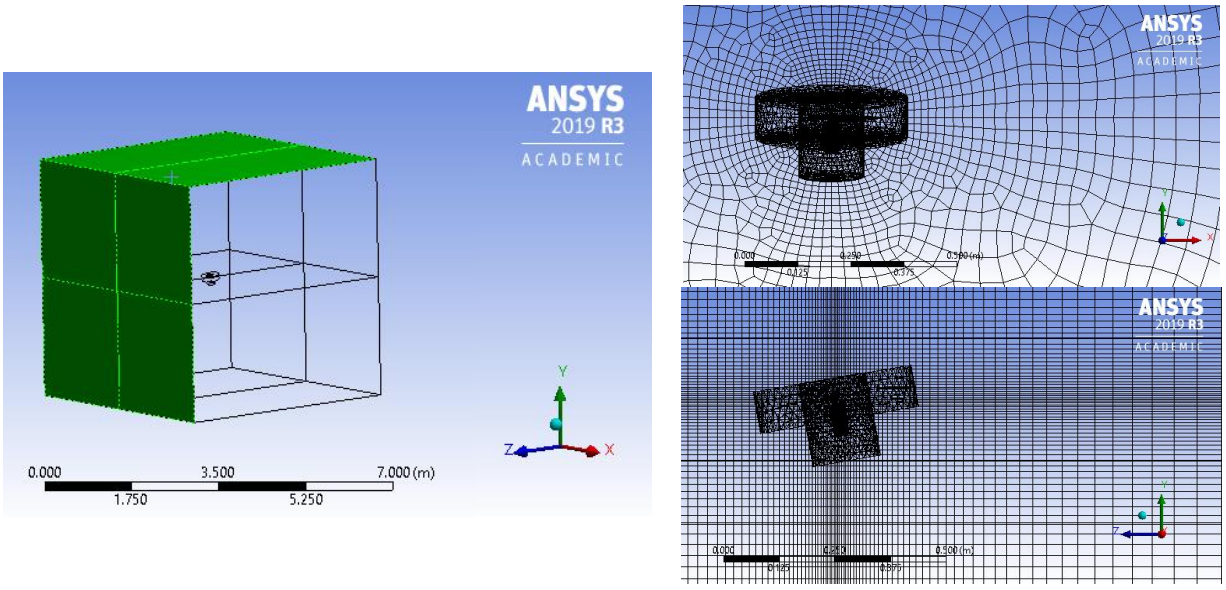

(a) (b)

Fig. 13 Meshes for simulation: (a) The velocity inlet boundaries of the Farfield mesh; (b) Rotating mesh and the nacelle at the center of the Farfield mesh in front (top) and side view (bottom).

From the velocity magnitude contour (Figure 14) and the plot of the velocity magnitude at 0.12 m and 0.18 m downstream from the propeller (Figure 15), the flow simulation is able to produce the two high velocity regions in the propeller's wake that appear in the PIV measurement from the experiment [21], albeit the velocity magnitude is overestimated in the simulation. The maximum velocity in the high velocity regions also occur slightly lower in the simulation than in the experiment. This may be due to a different angular velocity used for the rotating propellers as the angular velocity used in the experiment is not explicitly specified, such that higher RPM in the simulation can cause the high velocity regions to have higher velocity magnitude and be slightly lowered. The difference in the geometry built for the simulation with the supporting structure used in the experiment could also have affected the simulation results, as not all the supporting structure from the experiment is modelled for the simulation and there remains a small gap between the propeller and the nacelle in the simulation.

Additionally, in the velocity magnitude contour from the simulation shown in Figure 14(b), the contour for the region in between the two high velocity regions is not fully uniform in color due to the lack of cells in the propeller's wake region for the Farfield mesh and the interpolations during post-processing the simulation results. Improvement of the Farfield mesh by mesh adaptation in the propeller's wake region can be applied for future works to capture the flow from the propeller in more detail.

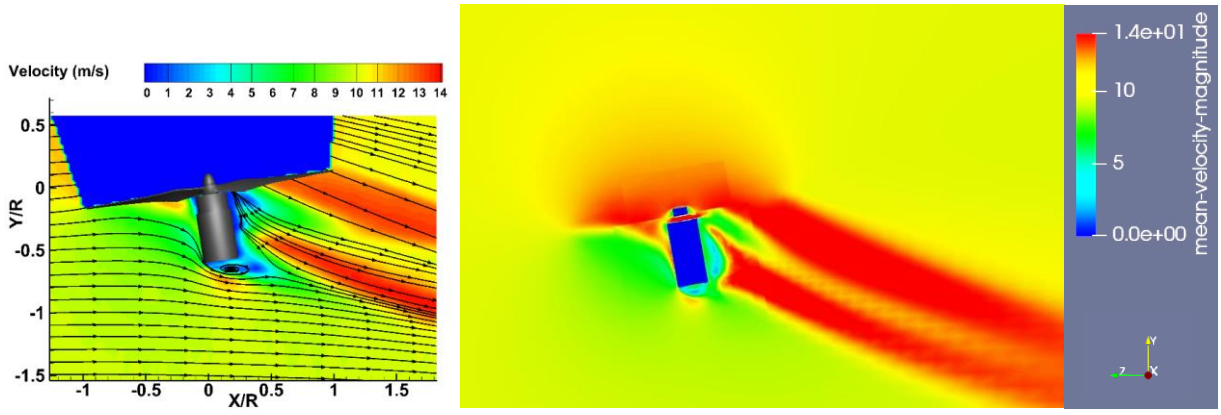

(a) (b)

Fig. 14 Velocity magnitude contour: (a) from PIV measurements [21]; (b) from simulation for a single propeller in forward flight condition.

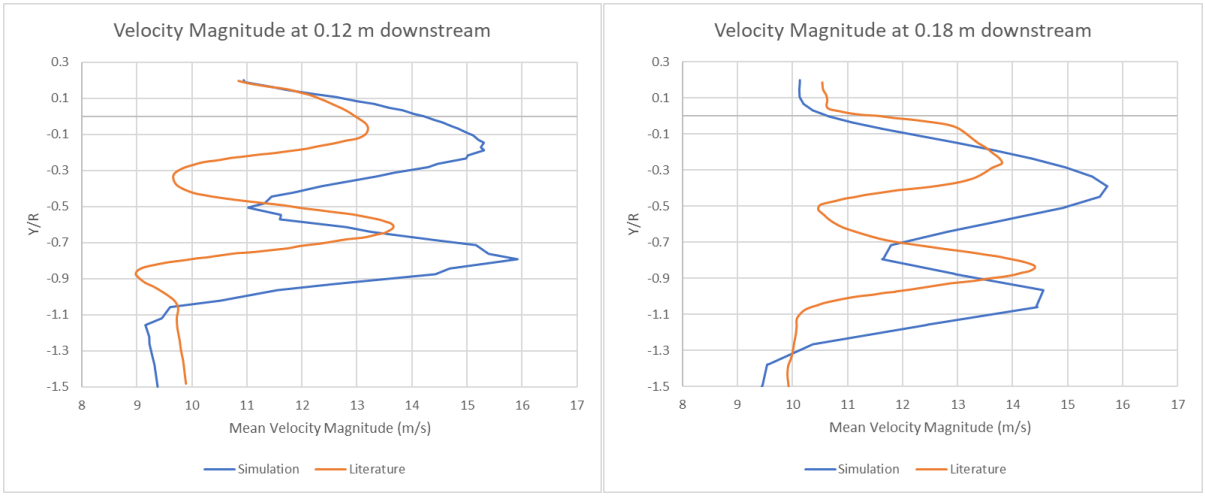

(a) (b)

Fig. 15 Velocity magnitude profile: (a) at 0.12 m; (b) at 0.18 m downstream from the propeller in forward flight condition.

VI. Conclusions

In this study, flow investigation of flying drones has been carried out for single and multiple quadrotor propellers in different flight conditions using the overset mesh on ANSYS Fluent 19.2. The study can help to establish safe separation and its boundary of drone operations. The CFD simulation results have been found to be in general agreement to the computational and experimental results that are available from other studies. This demonstrates that the CFD method presented here can be acceptably reliable in predicting the resulting airflow from quadrotor propellers and the method can be used as a tool to study the near-field, i.e. within one vehicle length, wake vortex induced by UAS.

Moving forward for the wake-encounter study, the simulation of far-field wake vortex will have to rely on employing LES model due to the dissipative nature of RANS-based turbulence models when it comes to vortical flow. Other future works should also include improvements in creating and setting up the meshes for the flow simulations to better capture the detailed flow from the rotating propellers; further applications of the CFD method to various cases of flying UAS, such as UAS of different sizes; UAS in various flight conditions such as cruising speed, tilt angle, rotor RPM, etc.; and different configurations of UAS such as with mainframe body, added landing gears, added payload, etc.

Acknowledgments

The authors would like to thank the Air Traffic Management Research Institute (ATMRI) for funding this research under the UAS Programme.

References

[1] Aydin, B. (2019). Public acceptance of drones: Knowledge, attitudes, and practice. *Technology in Society*, *59* (November 2017), 101180. https://doi.org/10.1016/j.techsoc.2019.101180

[2] Kaya, D., Turker Kutay, A., Funda Kurtulus, D., Tekinalp, O., Simsek, I., Soysal, S., & Hosgit, G. (2016). Propulsion system selection and modeling for a quadrotor with search and rescue mission. *54th AIAA Aerospace Sciences Meeting*, *January*, 1–10. https://doi.org/10.2514/6.2016-1528

[3] Wen, S., Han, J., Ning, Z., Lan, Y., Yin, X., Zhang, J., & Ge, Y. (2019). Numerical analysis and validation of spray distributions disturbed by quad-rotor drone wake at different flight speeds. *Computers and Electronics in Agriculture*, *166*(September), 105036. https://doi.org/10.1016/j.compag.2019.105036

[4] Throneberry, G., Hocut, C. M., Shu, F., & Abdelkefi, A. (2019). Multi-rotor wake propagation investigation for atmospheric sampling. *AIAA Aviation 2019 Forum*, *June*, 1–9. https://doi.org/10.2514/6.2019-3604

[5] Hwang, J., & Choe, J. Y. (Jacey). (2019). Exploring perceived risk in building successful drone food delivery services. *International Journal of Contemporary Hospitality Management*, *31*(8), 3249–3269. https://doi.org/10.1108/IJCHM-07-2018-0558

[6] Hochstenbach, M., Notteboom, C., Theys, B., & De Schutter, J. (2015). Design and control of an unmanned aerial vehicle for autonomous parcel delivery with transition from vertical take-off to forward flight - VertiKUL, a quadcopter tailsitter. *International Journal of Micro Air Vehicles*, *7*(4), 395–405. https://doi.org/10.1260/1756-8293.7.4.395

[7] Barbeau, Z. P., & Jacob, J. D. (2017). Flight test of small UAS wake vortex encounters - Part 1: Control system development and evaluation. *AIAA SciTech Forum - 55th AIAA Aerospace Sciences Meeting*, *January 2017*, 1–17. https://doi.org/10.2514/6.2017-0957

[8] Rossow, V., & James, K. (1999). Overview of wake-vortex hazards during cruise. In *17th Applied Aerodynamics Conference*. American Institute of Aeronautics and Astronautics. https://doi.org/doi:10.2514/6.1999-3197

[9] S. Teager, K. Biehl, L. Garodz, J. Tymczyszym, and D. Burnham. Flight test investigation of rotorcraft wake vortices in forward flight. Technical Report DOT/FAA/CT-94/117, FAA, 1996.

[10] Ferguson, S., & Dreier, M. E. (2005). Empirical wake turbulence model of tiltrotor aircraft. *SAE Technical Papers*, *724*. https://doi.org/10.4271/2005-01-3182

[11] Kutty, H. A., & Rajendran, P. (2017). 3D CFD simulation and experimental validation of small APC slow flyer propeller blade. *Aerospace*, *4*(1). https://doi.org/10.3390/aerospace4010010

[12] Pérez Gordillo, A. M., Santos, J. S. V., Lopez Mejia, O. D., Collazos, L. J. S., & Escobar, J. A. (2019). Numerical and experimental estimation of the efficiency of a quadcopter rotor operating at hover. *Energies*, *12*(2), 1–19. https://doi.org/10.3390/en12020261

[13] Kaya, D., Kutay, A. T., & Tekinalp, O. (2017). Experimental Investigation of Optimal Gap Distance between Rotors of a Quadrotor UAV. *AIAA Atmospheric Flight Mechanics Conference*, *June*, 1–9. https://doi.org/10.2514/6.2017-3894

[14] Zhou, W., Ning, Z., Li, H., & Hu, H. (2017). An experimental investigation on rotor-to-rotor interactions of small UAV. *35th AIAA Applied Aerodynamics Conference, 2017*, *June*, 1–16. https://doi.org/10.2514/6.2017-3744

[15] Shukla, D., & Komerath, N. (2018). Multirotor Drone Aerodynamic Interaction Investigation. *Drones*, *2*(4), 43. https://doi.org/10.3390/drones2040043

[16] Aleksandrov, D., & Penkov, I. (2012). Optimal gap distance between rotors of mini quadrotor helicopter. *Proceedings of the International Conference of DAAAM Baltic*, *April*, 251–255.

[17] Céspedes, J. F., & Lopez, O. D. (2019). Simulation and validation of the aerodynamic performance of a quadcopter in hover condition using overset mesh. *AIAA Aviation 2019 Forum*, *June*, 1–14. https://doi.org/10.2514/6.2019-2824

[18] Yoon, S., Lee, H. C., & Pulliam, T. H. (2016). Computational Analysis of Multi-Rotor Flows. *54th AIAA Aerospace Sciences Meeting*, 1–11. https://doi.org/10.2514/6.2016-0812

[19] Misiorowski, M., Gandhi, F., & Oberai, A. A. (2018). A computational study on rotor interactional effects for a quadcopter in edgewise flight. *Annual Forum Proceedings – AHS International*, *2018-May*. https://doi.org/10.2514/1.j058369

[20] Ventura Diaz, P., & Yoon, S. (2018). High-Fidelity Computational Aerodynamics of Multi-Rotor Unmanned Aerial Vehicles. *2018 AIAA Aerospace Sciences Meeting*, *210059*, 1–22. https://doi.org/10.2514/6.2018-1266

[21] Ning, Z., Wlezien, R., & Hu, H. (2018). EXPERIMENTAL INVESTIGATION ON THE SERRATED TRAILING EDGE PROPELLER OF SMALL UNMANNED AERIAL SYSTEM. *Experimental investigations on the aerodynamic and aeroacoustic characteristics of small UAS propellers*, 32. *Graduate Theses and Dissertations*. 16427. https://lib.dr.iastate.edu/etd/16427